nature reviews electrical engineering

https://doi.org/10.1038/s44287-026-00331-5

Supplementary information

Multidimensional optical singularities and their applications

In the format provided by the authors and unedited

Supplementary Information: Multidimensional optical singularities and their applications

Soon Wei Daniel Lim[1,2,†], Christina M. Spaegele[1,†], and Federico Capasso[1,*]

[1]Harvard John A. Paulson School of Engineering and Applied Sciences, Harvard University, Cambridge, MA 02138, USA
[2]Stanford University Department of Molecular and Cellular Physiology, Stanford, CA 94305, USA
[*]e-mail: capasso@seas.harvard.edu
[†]equal contribution

1 Mathematical nomenclature

Throughout, we use *unbolded* symbols (*e.g.,* ϕ, f) to denote scalars, which can either be complex ($\mathbb{C}$) or real-valued ($\mathbb{R}$). Vector symbols ($\vec{E}, \vec{H}$) represent column vectors and vector-valued functions, and overlined symbols ($\overline{J}$) indicate matrices and tensors.

Time-harmonic electromagnetic fields follow the convention $e^{i\omega t}$. The real and imaginary components of the complex number are written $E = E_r + iE_i$, $E_r = Re(E)$, and $E_i = Im(E)$. The intensity I of a scalar field is given by $|E|^2$, and the phase ϕ is the four-quadrant arctangent, $\phi = \text{atan2}(E_i, E_r)$. We choose the direction of propagation when it exists to be the longitudinal/axial z axis.

The transverse polarization vector $\vec{E}_\perp = (E_x, E_y)$ is known as the Jones vector. Transverse polarization can be described by the polarization ellipse on the transverse plane, which is parametrized by two variables: the azimuth Ψ, which is the angle that the major axis of the polarization ellipse makes with the transverse x-direction, and the ellipticity angle θ, which determines the eccentricity and handedness (right handed or left handed, based on the temporal path of the electric field vector) of the ellipse.

The transverse polarizations in the Jones vector can also be expressed in terms of the Stokes polarization parameters. These are four experimentally measurable intensities defined below using the left-handed convention[1].

$$S_0 = I_x + I_y = |E_x|^2 + |E_y|^2 \tag{1}$$

$$S_1 = I_x - I_y = |E_x|^2 - |E_y|^2 \tag{2}$$

$$S_2 = I_{45^\circ} - I_{-45^\circ} = 2\,\text{Re}(E_x E_y^*) \tag{3}$$

$$S_3 = I_{LCP} - I_{RCP} = 2\,\text{Im}(E_x E_y^*) \tag{4}$$

Here, I_j denotes the intensity of the polarization component projected in the j direction. For fully polarized light, $S_0^2 = S_1^2 + S_2^2 + S_3^2$, and for partially polarized light, $S_0^2 < S_1^2 + S_2^2 + S_3^2$. The fully polarized states thus lie on a sphere in (S_1, S_2, S_3) space, which is known as the Poincaré sphere. The Poincaré sphere perfectly unifies the Stokes parameter and polarization ellipse pictures: Lines of constant Ψ are longitudes on the sphere and lines of constant θ are the sphere's latitudes. The poles of the Poincaré sphere ($\theta = \pm\pi/2$) represent circularly polarized light of opposite handedness. Some texts define the ellipticity angle as half the latitude $\chi = \theta/2$, so the poles are at $\chi = \pm\pi/4$.

2 Optical fields as mappings

At every point of a D_{config}-dimensional configuration (parameter) space, the optical field assigns a set of $D_{condition}$ real-valued numbers, such as the real and imaginary parts of its Cartesian fields. We can say that optical fields are maps from configuration space to condition space $F : S_{config} \mapsto S_{condition}$. S_{config} is usually Cartesian space $S_{config} = \mathbb{R}^{D_{config}}$ for simplicity, but both S_{config} and $S_{condition}$ spaces just need to be differentiable manifolds; that is, they are spaces that locally resemble Euclidean space. Singularities are the positions in configuration space at which the $D_{condition}$ numbers are simultaneously zero; singular positions are the *preimage* in configuration space of the *origin* (all conditions zero) in condition space. For topological analysis, the mapping must explicitly exclude the preimage of the condition space zero, that is, it excludes the singular positions in configuration space. Therefore, the optical field is more rigorously described in topology as a continuous mapping between the configuration space in the vicinity of the singularity and the condition space in the vicinity of the origin. This restriction is necessary so that the mapping is globally well-defined and prevents the mapping from being continuously transformed into the singular point(s), which would otherwise allow a non-trivial topology to be unwound. Although this formalism may seem excessively convoluted when dealing with easily visualized structures in scalar fields, it becomes essential when handling vector-valued fields with high dimensional D_{config} and $D_{condition}$ spaces, such as singularities in the polarization field of light.

3 Topological charge for C and V loci

The topological charge for C loci is computed in a similar manner to phase singularities, since both singularities have a co-dimension of two. Consider a plane featuring a C polarization singularity at its center. At this singularity, the transverse polarization is strictly circular (or undefined), as that is the only condition that satisfies the condition set $\vec{E}_\perp \cdot \vec{E}_\perp = 0$ or $\vec{E} \cdot \vec{E} = 0$. Circular polarization means that the polarization azimuth is undefined. It was Freund who noted that the polarization azimuth Ψ could be expressed as half the complex angle of the Stokes field $\Sigma = S_1 + iS_2$ (Equation 5), with S_1 and S_2 being two of the real-valued Stokes parameters[2]. The Stokes field Σ is zero at the C locus itself $S_1 = 0, S_2 = 0$, thus the condition values are $\{S_1, S_2\}$.

$$\arg(\Sigma) = \arg(S_1 + iS_2) = 2\Psi \tag{5}$$

The topological invariant associated with C loci can thus be computed by a closed loop integral on a plane around the singularity.

$$l_C = \frac{1}{2\pi} \oint_S d^1\Omega = \frac{1}{2\pi} \oint_S \nabla atan2(S_2, S_1) \cdot d\vec{r}, l_C \in \mathbb{Z} \tag{6}$$

There is a distinction to be made in the definition of the C loci topological invariant as compared to those cited in the literature[2,3]. It is typically the accumulation of the azimuth Ψ that is used for this invariant calculation, instead of the angle subtended by $\{S_1, S_2\}$, which is 2Ψ. Ψ assumes values from $[0, \pi)$ rather than $[0, 2\pi)$, as a standard phase would, and accumulates half-integer and integer multiples of 2π on closed loops around the singularity. The reason is that the polarization azimuth does not have a pointing direction - it aligns with the semi-major axis of the polarization ellipse but remains invariant under a π rotation, thus still referring to the same polarization ellipse. Polarization azimuths that differ by an integer multiple of π are identical. Consequently, the topological invariant associated with accumulation of the polarization azimuth can take on both integer and half-integer values, whereas the topological invariant computed by accumulating $atan2(S_2, S_1)$ will only take integer values. In a 2D plane, generic C loci have three distinct topologies, named after their equivalent umbilical points: star ($I_C = -1/2$), monstar ($I_C = +1/2$), and lemon ($I_C = +1/2$)[3].

Just as phase singularities with $D_{config} = 2$ are structurally stable when their winding numbers are ± 1, a point singularity with co-dimension $D_{condition}$ and in a configuration space with $D_{config} = D_{condition}$ is structurally stable when its topological charge (obtained from the degree of continuous mapping) is ± 1. We can make this concrete by studying paraxial V loci, which occur when the transverse complex polarization fields vanish $E_{x,y} = 0$, a singularity with a co-dimension of four ($Re(E_x) = 0, Im(E_x) = 0, Re(E_y) = 0, Im(E_y) = 0$). To examine the structural stability of a point paraxial V locus, we need to identify a four-dimensional configuration space. As described in Spaegele et al[4], such a configuration space is the three dimensions of Cartesian space and one synthetic dimension of incident wavelength: (x, y, z, λ). Such singularities occur in configuration space when the fields map to the origin of condition space $\{Re(E_x), Im(E_x), Re(E_y), Im(E_y)\}$. To examine structural stability, we consider the mapping of the boundary 3-sphere surrounding the singularity in configuration space, which we will call S, to the 4D condition space:

$$l_4 = \frac{1}{2\pi^2} \oint_S d^3\Omega, l_4 \in \mathbb{Z} \tag{7}$$

$d^3\Omega$ is the differential solid angle for a 4D sphere, which has a total solid angle of $A = 2\pi^2$. When $l_4 = \pm 1$, all possible values of $Re(E_{x,y}), Im(E_{x,y})$ occur in the immediate vicinity of the singularity (up to overall normalization), which means that all complex transverse polarization fields (including the global phase) exist in the 4D configuration space around that singularity. Such a paraxial V locus is thus structurally stable against the perturbative influence of stray light of any transverse polarization.

4 Singularities required in eigenmode orthogonality

Orthogonality requires phase singularities to be present in the mode profiles. Orthogonality is the property that the inner product between two different eigenmodes is zero and strictly positive when evaluated for the same eigenmode, and this allows a linear combination of eigenmodes to be unambiguously decomposed into its constituent eigenmodes by taking its inner product with each member of an eigenmode set. For scalar modes that occupy the same space, *i.e.,* not spatially separated like in uncoupled many-core fibers, orthogonality requires that all but one of the scalar modes (usually the lowest-order mode) have field zero-crossings, which are zero lines or surfaces in 3D. To see this, consider the example of the inner product for two propagating real-valued scalar modes (indexed a and b) defined over a transverse xy region S (Equation 8):

$$\langle \phi_a | \phi_b \rangle = \iint_S w(\vec{r}) \phi_a(\vec{r}) \phi_b(\vec{r}) d^2\vec{r} \tag{8}$$

$w(\vec{r})$ is a non-negative weighting function. It is non-negative because of the requirement that $\langle \phi_a | \phi_a \rangle > 0$ for all eigenmodes $\{a\}$. We want to show that there is at most one eigenmode in an orthogonal basis that has no sign changes and thus no phase singularities. Assume the contrary; let there be more than one eigenmode in an orthogonal basis with no sign changes. Due to the continuity of physically realizable modes, each of these eigenmodes will have the same sign over S, and their product will also have the same sign over S. This means that $\langle \phi_a | \phi_b \rangle$ cannot be zero except for the case where one or more of the eigenmodes is zero everywhere or where the modes are located in disjoint spaces, such as angularly localized ANG modes[5]. In the former, these eigenmodes cannot be part of an orthogonal basis. We exclude the latter case where the modes are located in disjoint spaces since the modes do not superpose and just propagate through spatially separate channels. By contradiction, there is at most one eigenmode in an orthogonal set that has no sign changes; all other eigenmodes must have phase singularities.

5 Toraldo pupil synthesis

How can Toraldo pupil synthesis produce diffraction lobes that are narrower than the angular resolution limit of $1.22\lambda/D$ as expressed in the Rayleigh criterion? The Rayleigh criterion is an angular resolution bound for open, unstructured circular apertures and does not set an angular resolution limit for structured apertures. Supplementary Figure 2 provides a visual explanation of Toraldo synthesis. The main goal of the method is to enforce zero intensities at particular diffraction angles in the far field. We begin by dividing a circular pupil into multiple concentric zones. We would like to solve for the transmission amplitude associated with each pupil zone so that the pupil will produce the desired diffraction pattern in the far field. This transmission amplitude is a real number for amplitude-only masks and can be complex for masks with phase control. Each concentric ring produces a Bessel function (of the first kind) in the far field under uniform illumination, and the total far field diffraction pattern is the linear combination of these Bessel functions weighted by their respective (complex) amplitudes. Since there are N degrees of freedom for N concentric zones corresponding to their N amplitudes $A_1, \ldots, A_N$, we can solve for N independent constraints on the far field diffraction pattern. In effect, we are looking for an *interpolation* for a set of angle-intensity constraints in the far field diffraction pattern over the N individual ring diffraction patterns. The N unknowns and N constraints form a set of linear equations that can be solved numerically for $A_1, \ldots, A_N$. Schelkunoff and Toraldo di Francia's insight was that choosing these N constraints to be *zeros* of the diffracted field (red circles in Supplementary Figure 2) could "squeeze" the main lobe of the angular pattern so that it becomes smaller than that of the unstructured aperture. Additional zeros can then be added to move the large sidelobes away from the squeezed main lobe. For long wavelengths in the radio regime, enough zero positions can even push the sidelobes into the evanescent field with diffraction angles greater than $\pm\pi/2$, ensuring that the sidelobes do not propagate into the far field at all.

The central lobe in Toraldo synthesis can be made superoscillatory. The spatial frequencies in the far field diffraction pattern come from the off-axis zones of the illuminated pupil: zones or rings that are further away from the optic axis produce Bessel functions with higher spatial frequencies. The maximum spatial frequency in the far field of the pupil is determined by the diameter of the pupil; an infinitely thin ring with the same diameter as the pupil produces a Bessel function that has a central lobe full-width-at-half-maximum (FWHM) of $0.72\lambda/D$[6]. Thus, an engineered central lobe with a FWHM less than $0.72\lambda/D$ is superoscillatory.

The subdiffraction capabilities of Toraldo pupils come at a high cost: such supergain (super-directive in modern terminology) antennas with evanescent sidelobes require extremely high reactive currents and high current precision in the antenna elements, and these requirements become more stringent with higher gain. There is no theoretical upper limit to the gain of a supergain antenna; the limits come from the practicality of fabricating extremely precise antenna elements that can be strongly driven with precise currents[7].

6 Singularities in the canonical superoscillation function

It is sometimes unclear what role singularities play when the superoscillatory function itself does not contain any singularities. Consider the canonical superoscillation function, which is arguably the most studied superoscillatory function in the literature[8,9]:

$$f(x) = (\cos x + ia \sin x)^N, \quad x \in \mathbb{R} \tag{9}$$

where N is a large even integer and $a > 1$. The function's periodicity is π and it is bandlimited with wavenumbers $|k| \leq N$. The function's intensity and phase profile are plotted in Supplementary Figure 3a for $N = 20$ and $a = 10$. The function achieves very rapid phase variation near $x = 0$ and large sidebands away from it. The behavior of the function near $x = 0$ is plotted in Supplementary Figure 3b. The first order approximation for $f(x)$ near $x = 0$ is e^{iaNx}, thus it appears to have a large wavenumber aN despite being bandlimited to $|k| \leq N$. $a > 1$ can be considered the degree of superoscillation over the maximum frequency component. The function intensity $|f(x)|^2 = [1 + (a^2 - 1)\sin^2 x]^N$ is strictly positive over the real line, hence there are no zeros or singularities where $f(x) = 0$.

Supplementary Table 1. Classification of singular features. Classification of singular features, along with their defining mathematical properties and characteristic co-dimension (*i.e.,* number of conditions). $S_1 = |E_x|^2 - |E_y|^2, S_2 = 2\,\mathrm{Re}(E_x E_y^*)$ and $S_3 = 2\,\mathrm{Im}(E_x E_y^*)$ are three of the four Stokes parameters in the left-handed convention[1], where $S_0 = |E_x|^2 + |E_y|^2$ is the paraxial field intensity. $\vec{\sigma} \equiv (1/4\omega)[\varepsilon_0 Im(\vec{E}^* \times \vec{E}) + \mu_0 Im(\vec{H}^* \times \vec{H})]$ is the total spin angular momentum density, $\mu(r_1, r_2; \omega) = \langle E^*(r_1, \omega) E(r_2, \omega)\rangle$ is the cross-spectral density and $\Gamma(r_1, r_2; \tau) = \langle E^*(r_1, t) E(r_2, t+\tau)\rangle$ is the mutual coherence function.

Type	Singular parameter	Conditions	Co-dim.	Refs.
Phase	$\arg(E)$	$Re(E) = 0, Im(E) = 0$	2	10
Paraxial Disclination	Instantaneous transverse polarization	$E_x(t) = 0, E_y(t) = 0$	2	11
Paraxial C	Transverse polarization azimuth or $\arg(S_1 + iS_2)$	$S_1 = 0, S_2 = 0$	2	12, 13
Non-paraxial C	Vectorial polarization azimuth	$Re(\vec{E} \cdot \vec{E}) = 0, Im(\vec{E} \cdot \vec{E}) = 0$	2	14
Paraxial L	2D polarization ellipse normal	$S_3 = 0$	1	2, 11, 12, 15
Non-paraxial L	3D polarization ellipse normal vector	$\vec{E} \times \vec{E}^* = \vec{0}$	2	11, 14
Paraxial V	2D polarization ellipse	$\vec{E}_\perp = \vec{0}$, equivalently $Re(E_x) = Im(E_x) = Re(E_y) = Im(E_y) = 0$	4	2, 16
Non-paraxial V	3D polarization ellipse	$\vec{E} = \vec{0}$, equivalently $Re(E_x) = Im(E_x) = Re(E_y) = Im(E_y) = Re(E_z) = Im(E_z) = 0$	6	17–19
Spin defect	Spin angular momentum density	$\vec{\sigma} \equiv (\sigma_x, \sigma_y, \sigma_z) = \vec{0}$	3	20
Cross-spectral density	$\arg(\mu)$	$Re(\mu) = 0, Im(\mu) = 0$	2	21
Mutual coherence function	$\arg(\Gamma)$	$Re(\Gamma) = 0, Im(\Gamma) = 0$	2	22

When the canonical superoscillation function is plotted over the complex plane instead of just the real line (that is, allowing x to be complex instead of purely real), the reason for the superoscillatory behavior of $f(x)$ immediately becomes clear. Supplementary Figures 3(c-d) plot the intensity and phase profile of $f(x)$ over the complex plane for x, respectively. Although the real line does not pass through any singularities, there is a phase singularity located at a distance of $\sinh^{-1}[(a^2-1)^{-1/2}]$ above the real axis, producing a reduced function intensity along the real line around $Re(x) = 0$. Importantly, the phase singularity is a *vortex singularity* with a topological charge $l = N$. These complex plane images demonstrate the wider context around the 1D superoscillatory function, demonstrating that its rapid phase variation and low intensity near $Re(x) = 0$ are simply due to its proximity to a charge N vortex phase singularity located in the *imaginary direction*! Increasing the degree of superoscillation a decreases the distance $\sinh^{-1}[(a^2-1)^{-1/2}]$ to the phase singularity, thereby decreasing the minimum intensity and also increasing the maximum phase gradient along the real axis. Changing the value of the integer N simply changes the number of 2π phase windings around the vortex core, thereby changing the number of 2π phase wrappings along the real line of the function. Even though the canonical superoscillation function does not pass through any singularities on its domain of the real line, its superoscillatory properties are still derived from its proximity to a phase singularity, albeit in the complex plane.

7 Supplementary Figures

References

1. Collett, E. *Polarized light: fundamentals and applications* (Marcel Dekker, 1993).
2. Freund, I. Polarization singularity indices in Gaussian laser beams. *Opt. Commun.* **201**, 251–270, DOI: 10.1016/S0030-4018(01)01725-4 (2002).
3. Nye, J. F. Lines of circular polarization in electromagnetic wave fields. *Proc. Royal Soc. London. A. Math. Phys. Sci.* **389**, 279–290, DOI: 10.1098/rspa.1983.0109 (1983).
4. Spaegele, C. M. *et al.* Topologically protected optical polarization singularities in four-dimensional space. *Sci. Adv.* **9**, eadh0369, DOI: 10.1126/sciadv.adh0369 (2023).
5. Mirhosseini, M. *et al.* High-dimensional quantum cryptography with twisted light. *New J. Phys.* **17**, 033033, DOI: 10.1088/1367-2630/17/3/033033 (2015).
6. Grosjean, T. & Courjon, D. Smallest focal spots. *Opt. Commun.* **272**, 314–319, DOI: 10.1016/j.optcom.2006.11.043 (2007).

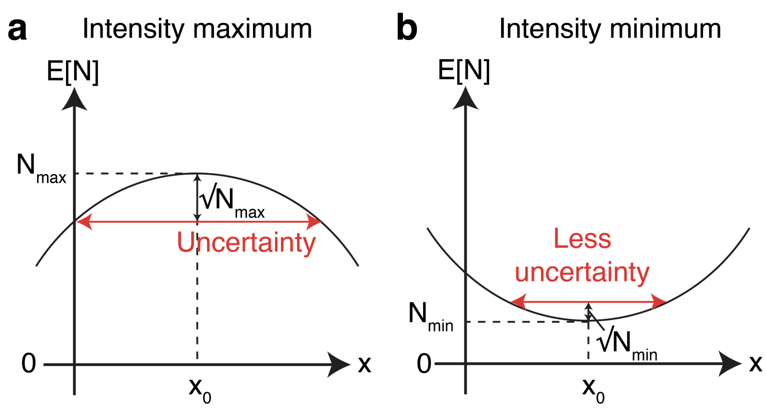

Supplementary Figure 1. **Model for the localization precision of an intensity maximum versus intensity zero**. The uncertainty in a localization measurement is the range in x position that is consistent with a signal within one standard deviation $\sqrt{N}$ of the feature signal strength N. **a** An intensity maximum has a higher central intensity compared to that of the intensity minimum $N_{max} \gg N_{min}$. Thus, it has a large intensity standard deviation and a large positional uncertainty. **b** An intensity minimum has a small minimum intensity and thus has a reduced localization error. For a phase singularity, N_{min} can be made near zero. Image adapted from J. Xiao and T. Ha, Flipping nanoscopy on its head, Science 355, 582–584 (2017)[29]. Adapted with permission from AAAS.

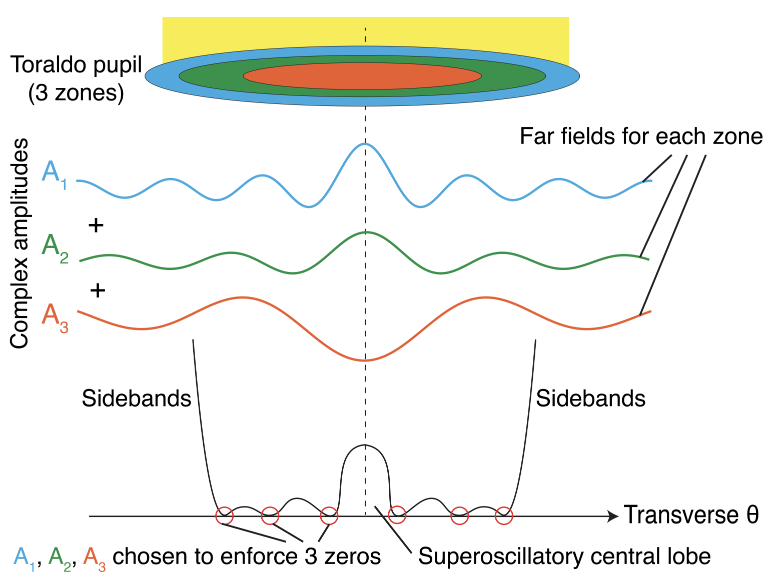

Supplementary Figure 2. Toraldo synthesis of a superoscillatory spot in the far field, which can be used to construct super-directive antennas. A Toraldo pupil comprises various concentric zones. Each zone is associated with a complex or real-valued amplitude, depending on whether phase or amplitude masks are used. The far field diffraction pattern can be written as the sum of the individual zone diffraction patterns, weighted by their respective amplitudes. By enforcing zeros in the far field pattern, the central diffraction lobe can be squeezed until it is superoscillatory and has a characteristic width smaller than the diffraction limit. The cost is that large sidebands will form outside the superoscillatory region.

Supplementary Table 2. Relationship between singularity dimension, configuration space dimension and number of conditions. The singularity dimension is determined by the difference of configuration space dimension and the number of conditions that need to be fulfilled. The number in square brackets [] indicates the respective dimension of generic singularities with that combination of configuration dimension and singularity co-dimension. [0D] indicates points, [1D] indicates lines, [2D] indicates surfaces, and [3-5] indicates 3D or higher dimensional geometries. Cells without the square brackets do not have structurally stable singularities as the condition space dimension exceeds the configuration space dimension. Singularities with configuration space dimension exceeding 3 can use synthetic dimensions since there are only three Cartesian dimensions.

	Co-dim=1	**Co-dim=2**	**Co-dim=3**	**Co-dim=4**	**Co-dim=5**	**Co-dim=6**
Config. dim=1	[0D]					
Config. dim=2	[1D] L-line (paraxial L)[2]	[0D] Phase[10], c-point (paraxial C)[2,13,15], d point (paraxial disclination)[15]				
Config. dim=3	[2D] S-surface (paraxial L)[12]	[1D] C-line (paraxial C)[12], C^T line (non-paraxial C)[14], L^T line (non-paraxial L)[14]	[0D] Spin defect[20]	V-points (paraxial V)[2,16]		3D hollow spots (non-paraxial V)[18,19,23–28]
Config. dim=4	[3D]	[2D]	[1D]	[0D] Complete phase/pol. singularity (paraxial V)[4]		
Config. dim=5	[4D]	[3D]	[2D]	[1D]	[0D]	
Config. dim=6	[5D]	[4D]	[3D]	[2D]	[1D]	[0D]

7. Toraldo di Francia, G. Super-gain antennas and optical resolving power. *Il Nuovo Cimento* **9**, 426–438, DOI: 10.1007/BF02903413 (1952).

8. Berry, M. V. & Popescu, S. Evolution of quantum superoscillations and optical superresolution without evanescent waves. *J. Phys. A: Math. Gen.* **39**, 6965–6977, DOI: 10.1088/0305-4470/39/22/011 (2006).

9. Berry, M. *et al.* Roadmap on superoscillations. *J. Opt.* **21**, 053002, DOI: 10.1088/2040-8986/ab0191 (2019).

10. Nye, J. F. & Berry, M. Dislocations in wave trains. *Proc. Royal Soc. A: Math. Phys. Eng. Sci.* **336**, 165–190, DOI: 10.1098/rspa.1974.0012 (1974).

11. Nye, J. F. Polarization effects in the diffraction of electromagnetic waves: the role of disclinations. *Proc. Royal Soc. London. A. Math. Phys. Sci.* **387**, 105–132, DOI: 10.1098/rspa.1983.0053 (1983).

12. Hajnal, J. V. Singularities in the transverse fields of electromagnetic waves. I. Theory. *Proc. Royal Soc. London. A. Math. Phys. Sci.* **414**, 433–446, DOI: 10.1098/rspa.1987.0153 (1987).

13. Berry, M. V. Circular lines of circular polarization in three dimensions, and their transverse-field counterparts. *J. Opt.* **15**, 044024, DOI: 10.1088/2040-8978/15/4/044024 (2013).

14. Nye, J. & Hajnal, J. The wave structure of monochromatic electromagnetic radiation. *Proc. Royal Soc. London. A. Math. Phys. Sci.* **409**, 21–36, DOI: 10.1098/rspa.1987.0002 (1987).

15. Hajnal, J. V. Singularities in the transverse fields of electromagnetic waves. II. Observations on the electric field. *Proc. Royal Soc. London. A. Math. Phys. Sci.* **414**, 447–468, DOI: 10.1098/rspa.1987.0154 (1987).

16. Freund, I. Polarization flowers. *Opt. Commun.* **199**, 47–63, DOI: 10.1016/S0030-4018(01)01533-4 (2001).

17. Arlt, J. & Padgett, M. J. Generation of a beam with a dark focus surrounded by regions of higher intensity: the optical bottle beam. *Opt. Lett.* **25**, 191–193, DOI: 10.1364/OL.25.000191 (2000).

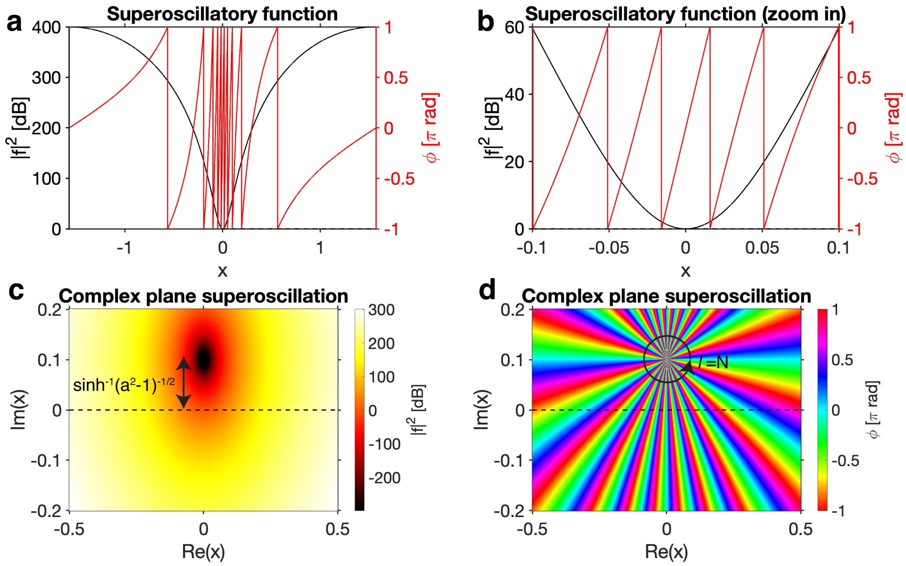

Supplementary Figure 3. The canonical superoscillation function $f(x) = (\cos x + ia\sin x)^N$ is bandlimited to $|k| \leq N$ (shortest wavelength $2\pi/N$) and derives its superoscillatory behavior from nearby singularities in complex space. In this figure, $a = 10, N = 20$. **a** The canonical superoscillation function plotted on its periodic real domain of $x \in [-\pi/2, \pi/2]$ shows rapid phase accumulation behavior near $x = 0$. **b** Zooming into the region near $x = 0$, the function has a phase accumulation like $\exp(iNax)$, which is $a = 10$ times more rapid than its spatial frequency bandlimit. The function does not vanish anywhere on the real line and so has no singularities on the real line. **c**-**d** The phase singularity responsible for the superoscillatory behavior is revealed when x is allowed to be complex. The **c** intensity and **d** phase profiles of the complex plane superoscillation are plotted. A vortex singularity with topological charge $l = N$ is located at a distance of $\sinh^{-1}[(a^2-1)^{-1/2}]$ above the real axis. The larger the value of a, the closer the singularity is to the real axis, which increases the phase gradient along the real axis.

18. Bokor, N. & Davidson, N. Generation of a hollow dark spherical spot by 4pi focusing of a radially polarized laguerre-gaussian beam. *Opt. Lett.* **31**, 149–151, DOI: 10.1364/OL.31.000149 (2006).

19. Kozawa, Y. & Sato, S. Focusing property of a double-ring-shaped radially polarized beam. *Opt. Lett.* **31**, 820–822, DOI: 10.1364/OL.31.000820 (2006).

20. Wang, H., Wojcik, C. C. & Fan, S. Topological spin defects of light. *Optica* **9**, 1417–1423, DOI: 10.1364/OPTICA.474612 (2022).

21. Schouten, H. F., Gbur, G., Visser, T. D. & Wolf, E. Phase singularities of the coherence functions in Young's interference pattern. *Opt. Lett.* **28**, 968–970, DOI: 10.1364/OL.28.000968 (2003).

22. Maleev, I. D., Palacios, D. M., Marathay, A. S. & Grover A. Swartzlander, J. Spatial correlation vortices in partially coherent light: theory. *J. Opt. Soc. Am. B* **21**, 1895–1900, DOI: 10.1364/JOSAB.21.001895 (2004).

23. Bokor, N. & Davidson, N. Tight parabolic dark spot with high numerical aperture focusing with a circular π phase plate. *Opt. Commun.* **270**, 145–150, DOI: 10.1016/j.optcom.2006.09.022 (2007).

24. Xue, Y., Kuang, C., Hao, X., Gu, Z. & Liu, X. A method for generating a three-dimensional dark spot using a radially polarized beam. *J. Opt.* **13**, 125704, DOI: 10.1088/2040-8978/13/12/125704 (2011).

25. Li, S., Kuang, C., Hao, X., Gu, Z. & Liu, X. Generation of a 3D isotropic hollow focal spot for single-objective stimulated emission depletion microscopy. *J. Opt.* **14**, 085704, DOI: 10.1088/2040-8978/14/8/085704 (2012).

26. Wan, C. *et al.* Three-dimensional visible-light capsule enclosing perfect supersized darkness via antiresolution. *Laser & Photonics Rev.* **8**, 743–749, DOI: 10.1002/lpor.201400006 (2014).

27. Wu, Z. *et al.* Generating a three-dimensional hollow spot with sub-diffraction transverse size by a focused cylindrical vector wave. *Opt. Express* **26**, 7866–7875, DOI: 10.1364/OE.26.007866 (2018).

28. Lim, S. W. D. *et al.* Point singularity array with metasurfaces. *Nat. Commun.* **14**, 3237, DOI: 10.1038/s41467-023-39072-6 (2023).

29. Xiao, J. & Ha, T. Flipping nanoscopy on its head. *Science* **355**, 582–584, DOI: 10.1126/science.aam5409 (2017).